第 31 卷第 11 期 无 机 化 学 学 报 Vol.31 No.11
2015 年 11 月 CHINESE JOURNAL OF INORGANIC CHEMISTRY 2111-2118

基于一种柔性二羧酸和不同双咪唑配体构筑的两例钴–穿插网格

杨玉亭* 屠长征 缪娇娇 李俊莉 陈 广
(曲靖师范学院化学化工学院,曲靖 655011)

摘要: 利用一种柔性二羧酸, 辅以不同的双咪唑配体在水热条件下构筑了两例具有穿插特征的钴配位聚合物,{[Co(bimb)(L)]·H_2O}$_n$(**1**)和{[Co(bbix)(L)]$_2$}$_n$(**2**)(H_2L=4,4′-(2,2′-oxybis(ethane-2,1-diyl)bis(oxy))dibenzoic acid, bimb=1,1′-(1,4-butanediyl)bis(imidazole), bbix=1,4-bis(benzimidazole-1-ylmethyl)-benzene)。单晶 X-射线衍射研究发现配合物 **1** 为 2D→3D 4-连 **sql** 拓扑构型的三重穿插网格;配合物 **2** 为 3D 4-连 6^6 **dia** 拓扑构型的六重穿插网格。该结构分析结果表明作为辅助配体的双咪唑配体的构型对配合物的穿插特征有重要影响。另外,我们还研究了配合物 **1** 和 **2** 的热稳定性及磁性。

关键词: 穿插; 柔性; 双咪唑; 拓扑; 磁性
中图分类号: O614.81+2 **文献标识码**: A **文章编号**: 1001-4861(2015)11-2111-08
DOI: 10.11862/CJIC.2015.291

Two Different Co(Ⅱ) Interpenetrating Networks Based on a Flexible Dicarboxylic Acid and Different Bis(imidazole) Ligands

YANG Yu-Ting* TU Chang-Zheng MIAO Jiao-Jiao LI Jun-Li CHEN Guang
(*College of Chemistry and Chemical Engineering, Qujing Normal University, Qujing, Yunnan* 655011, *China*)

Abstract: Two interpenetrating networks, namely {[Co(bimb)(L)]·H_2O}$_n$(**1**) and {[Co(bbix)(L)]$_2$}$_n$(**2**) (H_2L=4,4′-(2,2′-oxybis(ethane-2,1-diyl)bis(oxy))dibenzoic acid, bimb=1,1′-(1,4-butanediyl)bis(imidazole), bbix=1,4-bis(benzimidazole-1-ylmethyl)-benzene) have been prepared under hydrothermal condition by varying the bis (imidazole) coligands. Single crystal X-ray diffraction indicates that complex **1** displays 2D→3D 3-fold interpenetrating framework with 4-connected **sql** topology; **2** shows a 3D 4-connected framework of 6^6 **dia** topology with 6-fold interpenetration. The results indicate that the shapes of bis(imidazole) coligands have an important effect on the interpenetrating characters and ultimate frameworks. Moreover, the thermal and magnetic properties of the two complexes have also been studied. CCDC: 1413620, **1**; 1413621, **2**.

Key words: interpenetration; flexible; bis(imidazole); topology; magnetic properties

0 Introduction

Over the past few years, more and more attention has been devoted to the interpenetrating nets because of their undisputed beauty and particular functions. Up to now, a large number of beautiful interpenetrating nets have been reported, and also there are some comprehensive reviews by Robson, Batten, and Cianis groups[1-5]. Conceptually, interpenetrating networks can be described as a number of individual nets

收稿日期:2015-08-04。收修改稿日期:2015-09-22。
云南省科技厅应用基础研究项目(No.201401CB00299)资助。
*通讯联系人。E-mail:18288438002@163.com;会员登记号:S06N2384M1506。

participating in interpenetration with each other. Such peculiar structural character of interpenetrating networks can enhance the skeleton rigidity and interlattice interactions, thus creating materials with unique properties or functions, such as superhard materials, magnetic materials and highly stable materials[6-10]. Although the investigation on the interpenetrating nets advanced rapidly, the factors that control the observed degrees of interpenetration in these systems remain largely uncertain. In literature, the flexible or semirigid multicarboxylate and bis(imidazole) ligands have been extensively adopted to construct the high-dimensional interpenetrating networks, because of their varied coordination modes, abundant structural motifs, and flexible molecular backbones[11-13].

4,4′-(2,2′-oxybis(ethane-2,1-diyl)bis(oxy))dibenzoic acid (H_2L), as a long flexible dicarboxylic acid, should be an excellent candidate for constructing the interpenetrating networks due to the flexible nature of the two $(-O-CH_2-)_2$ spacers between the two phenyl rings. Besides, the $(-O-CH_2-)_2$ linker will cause the carboxyl groups to connect metal ions in different directions, offering various possibilities for construction of frameworks with unique structures and useful properties. For example, the reported complexes $\{[Zn(bpib)_{0.5}(L^4)]\}_n$ and $\{[Cd(bib)(L^4)]\}_n$ exhibit 2D→2D 3-fold interpenetrating network and 5-fold interpenetrating (4,4)-connected 2D wavy layers, respectively, and both of them possessing luminescent properties (bpib=1,4-bis(2-(pyridin-2-yl)-1*H*-imidazol-1-yl)butane, bib=1,4-bis(1*H*-imidazol-1-yl)butane, L^4= 4, 4′-(2,2′-oxybis(ethane-2, 1-diyl)bis(oxy))dibenzoic acid)[14]. However, only a few of interpenetrating nets based on the mixed H_2L and bis (imidazole) ligands have been crystallographically characterized so far[14-16]. The results of the combination of the flexible H_2L and bis (imidazole) ligands with 3*d* metal ions still attracting our attention.

Based on above consideration, our synthetic strategy is to select H_2L, and different bis(imidazole) ligands, *viz*. 1,1′-(1,4-butanediyl)bis(imidazole) (bimb) and 1,4-bis (benzimidazole-1-ylmethyl)-benzene (bbix) as organic linkers (Scheme 1), to construct interpenetrated networks. Fortunately, two novel entangled complexes $\{[Co(bimb)(L)]\cdot H_2O\}_n$(**1**) and $\{[Co(bbix)(L)]_2\}_n$(**2**) were successfully isolated. Notably, **1** and **2** are stable in the solid state upon extended exposure to air, and they have poor solubility in common organic solvents at room temperature, such as alcohol, acetonitrile, DMF, DMA and DMSO. Both **1** and **2** have been characterized by infrared spectroscopy, and elemental analysis. Thermogravimetric analysis, X-ray powder diffraction and magnetic susceptibility measurements were also investigated.

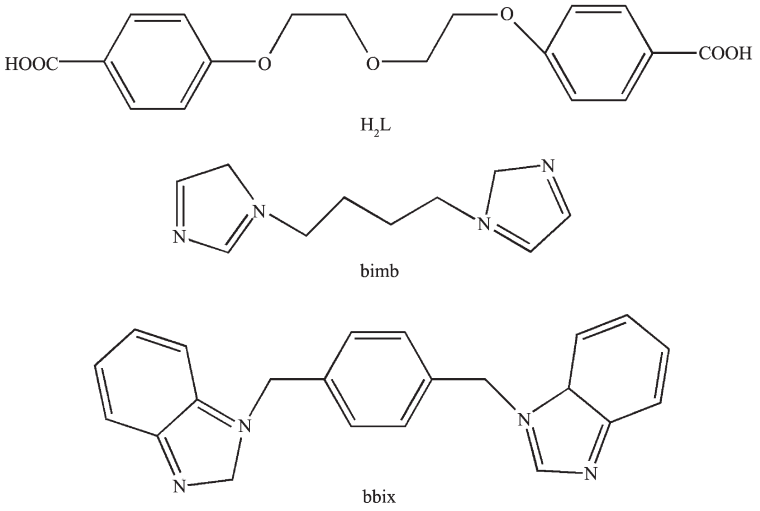

Scheme 1 Structures of H_2L and the N-donor ligands used in this work

1 Experimental

1.1 Materials and measurements

All the chemical regents were purchased commercially and were used as received without further purification. The ligands bimb and bbix were prepared according to reported procedures [17]. Elemental analyses for C, H, and N were performed on a Perkin-Elmer 240 analyzer. IR spectra were recorded as KBr pellets on a Nicolet Magna-FTIR 560 spectrometer in the 4 000 ~400 cm^{-1} regions. The magnetic measurements were performed on the Quantum Design SQUID MPMS XL-7 instruments in a magnetic field of 1 000 Oe in the temperature range of 2 ~300 K. The thermogravimetric analyses were investigated on a standard TG analyzer under a nitrogen flow at a heating rate of 5 ℃·min^{-1} for all measurements.

1.2 Preparation of complex 1

A mixture of $CoCl_2·6H_2O$ (0.2 mmol, 0.048 g), H_2L (0.2 mmol, 0.071 g) and bimb (0.2 mmol, 0.038 g) was placed in a Teflon-lined stainless steel vessel (23 mL), adjusting pH value to 6.0 by addition of Na_2CO_3 (0.05 mmol, 0.055 g), and was heated at 160 ℃ for 72 h. After the sample was gradually cooled to room temperature at the rate of 5 ℃·h^{-1}, deep purple crystals of **1** were obtained with 58% yield based on Co. Anal. Calcd. for **1** ($C_{28}H_{32}CoN_4O_8$) (%): C 54.99, H 5.27, N 9.16. Found (%): C 54.87 H 5.15, N 9.02. Selected IR data (KBr pellet, cm^{-1}): 3 304 (w), 1 608 (s), 1 307 (m), 1 094 (m), 1 053 (s), 941 (m), 784 (s), 656 (s), 730 (s).

1.3 Preparation of complex 2

The synthesis procedure of complex **2** was similar to that of complex **1** except that bimb was replaced by bbix. Purple block-shaped crystals of **2** were obtained with 63% yield based on Co. Anal. Calcd. for **2** ($C_{80}H_{68}Co_2N_8O_{14}$)(%): C 64.78, H 4.62, N 7.55. Found (%): C 64.71, H 4.49, N 7.43. Selected IR data (KBr pellet, cm^{-1}): 1 605 (s), 1 560 (m), 1 507 (m), 1 384 (s), 1 249 (m), 1 168 (s), 1 058 (m), 921 (m), 851 (m), 785 (m), 741 (s), 655 (s), 639 (m).

1.4 X-ray crystallography and structure determination

The well-shaped single crystals of complexes **1** and **2** were selected for X-ray diffraction study. The unit cell parameters and intensity data were collected at 293 K on a Bruker SMART APEX Ⅱ CCD diffractometer using a graphite-monochromated Mo-$K\alpha$ (λ =0.071 073 nm) radiation. The structures were solved by direct method using SHELXS program of the SHELXTL-97 package and refined by full-matrix least-squares fitting on F^2 by SHELX-97[18]. All non-hydrogen atoms were refined anisotropically, and the hydrogen atoms of organic ligands were located by geometrically. Crystal data and structure refinement parameters for **1** and **2** are summarized in Table 1. Selected bond distances and angles are listed in Table 2 and 3.

CCDC: 1413620, **1**; 1413621, **2**.

Table 1　Crystallographic Data for 1 and 2

Complex	**1**	**2**
Empirical Formula	$C_{28}H_{32}CoN_4O_8$	$C_{80}H_{68}Co_2N_8O_{14}$
Formula weight	611.51	1 483.28
Crystal system	Orthorhombic	Orthorhombic
Space group	*Pbca*	$P2_12_12_1$
a / nm	1.528 8(3)	1.503 7(3)
b / nm	1.754 6(4)	1.907 5(4)
c / nm	2.171 3(4)	2.490 1(5)
V / nm^3	5.824(2)	7.142(2)
Z	8	4
D_c / (g·cm^{-3})	1.395	1.379

Continued Table 1

μ / mm^{-1}	0.644	0.537
F(000)	2 552	3 080
Crystal size / mm	0.25×0.23×0.20	0.21×0.20×0.19
θ range / (°)	3.05~25.01	3.00~25.01
Limiting indices (h, k, l)	−18~18, −20~19, −25~25	−17~16, −22~21, −29~29
Reflections collected /unique	42 306 / 5 122	46 653 / 12 305
Observed reflections	3 054	6 779
Data / restrains / parameters	5 122 / 3 / 370	12 305 / 51 / 944
Goodness-of-fit on F^2	1.033	1.034
Final R indices [$I>2\sigma(I)$]	R_1=0.057 0, wR_2=0.109 0	R_1=0.060 4, wR_2=0.098 2
R indices (all data)	R_1=0.109 2, wR_2=0.126 4	R_1=0.126 6, wR_2=0.115 8
Largest diff. peak and hole / (e·nm^{-3})	404 and −278	197 and 297

Table 2 Selected bond lengths (nm) and bond angles (°) for complex 1

Co(1)-O(1)	0.196 9(3)	Co(1)-O(3)	0.193 9(3)	Co(1)-N(1)	0.202 4(3)
Co(1)-N(3)	0.199 9(3)				
O(3)-Co(1)-O(1)	105.61(12)	O(3)-Co(1)-N(3)	118.76(13)	O(1)-Co(1)-N(3)	119.99(12)
O(3)-Co(1)-N(1)	106.74(14)	O(1)-Co(1)-N(1)	101.41(12)	N(3)-Co(1)-N(1)	102.04(13)

Table 3 Selected bond lengths (nm) and bond angles (°) for complex 2

Co(1)-O(8)	0.194 2(5)	Co(1)-O(14)a	0.197 0(4)	Co(1)-N(1)	0.201 5(5)
Co(1)-N(6)	0.202 1(5)	Co(2)-O(4)	0.194 4(4)	Co(2)-O(2)b	0.194 5(5)
Co(2)-N(7)	0.201 6(5)	Co(2)-N(4)c	0.202 5(5)	N(4)-Co(2)d	0.202 5(4)
O(2)-Co(2)e	0.194 5(5)	O(14)-Co(1)f	0.197 0(4)		
O(8)-Co(1)-O(14)a	97.8(2)	O(8)-Co(1)-N(1)	119.0(2)	O(14)a-Co(1)-N(1)	122.8(2)
O(8)-Co(1)-N(6)	114.4(2)	O(14)a-Co(1)-N(6)	100.8(2)	N(1)-Co(1)-N(6)	101.35(19)
O(4)-Co(2)-O(2)b	98.3(2)	O(4)-Co(2)-N(7)	99.3(2)	O(2)b-Co(2)-N(7)	115.3(2)
O(4)-Co(2)-N(4)c	120.5(2)	O(2)b-Co(2)-N(4)c	119.6(2)	N(7)-Co(2)-N(4)c	102.78(19)

Symmetry codes: a: $-x-1/2, -y, z+1/2$; b: $-x+5/2, -y, z+1/2$; c: $x, y-1, z$; d: $x, y+1, z$; e: $-x+5/2, -y, z-1/2$; f: $-x-1/2, -y, z-1/2$

2 Results and discussion

2.1 Structural description of 1

Single crystal X-ray analysis reveals that complex **1** crystallizes in the orthorhombic space group *Pbca*. The asymmetric unit consists of one independent Co(Ⅱ) ion, one L^{2-} anion, one bimb ligand, and one free water molecule. As shown in Fig.1a, each Co(Ⅱ) center is coordinated by two nitrogen atoms (N1 and N3) from two different bimb ligands, and two carboxylic oxygen atoms (O1 and O3) from two different L^{2-} anions, forming a slightly distorted CoO_2N_2 tetrahedron. The bond angles around each Co(Ⅱ) ion range from 101.41(12)° to 119.99(12)°. The Co-N bond distances are 0.202 4(3) (Co-N1) and 0.199 9(3) (Co-N3) nm, and the Co-O bond lengths are 0.196 9(3) (Co1-O1) and 0.193 9(3) nm (Co1-O3), respectively, which are similar to those found in other related cobalt complexes[19].

Each bimb ligand shows *trans* conformation with

dihedral angle of two imidazole rings being 6.02°. As shown in Fig.1b, the completely deprotonated L ligand acts as a μ_2-bridge linking two Co(Ⅱ) ions, in which each carboxylic group adopts the μ_1-η^1:η^0 bridging mode to connect the Co(Ⅱ) ions. The adjacent Co(Ⅱ) ions are bridged by L^{2-} anions to give 1D left- and right-handed helical chains $(CoL)_n$ along *c* direction, and the pitch of the helices is 2.171 3 nm. It is worth noting that the L ligands and metal ions usually forming loops in the reported complexes rather than helical chains. Furthermore, these helical chains are combined together by the bimb ligands to generate a 2D undulated layer with a large grid, showing the dimension of 1.159 2 nm×1.781 3 nm (Fig.1c).

From the viewpoint of network topology, the Co1 ions can be treated as 4-connected nodes, both L and bimb ligands can be regarded as linkers between the Co1 centers. Thus, the structure of **1** can be simplified as a uninodal 4-connected **sql** network with the Schläfli notation of $(4^4\cdot6^2)$ (Fig.1d). Based on the large grid in the layer, the other two identical layers penetrate it in the parallel mode ("above" and "below") to form a 2D→2D 3-fold interpenetrating network (Fig.1e). To our knowledge, such 2D→3D 3-fold interpenetrating network based on the 4-connected **sql** network is very rare.

2.2 Structural description of 2

To investigate the influence of the bis(imidazole) ligand on the structure of the complexes, the reaction of bbix and H_2L with $CoCl_2\cdot6H_2O$ was carried out, and a new complex **2** was obtained. Single crystal X-ray analysis reveals that complex **2** crystallizes in the

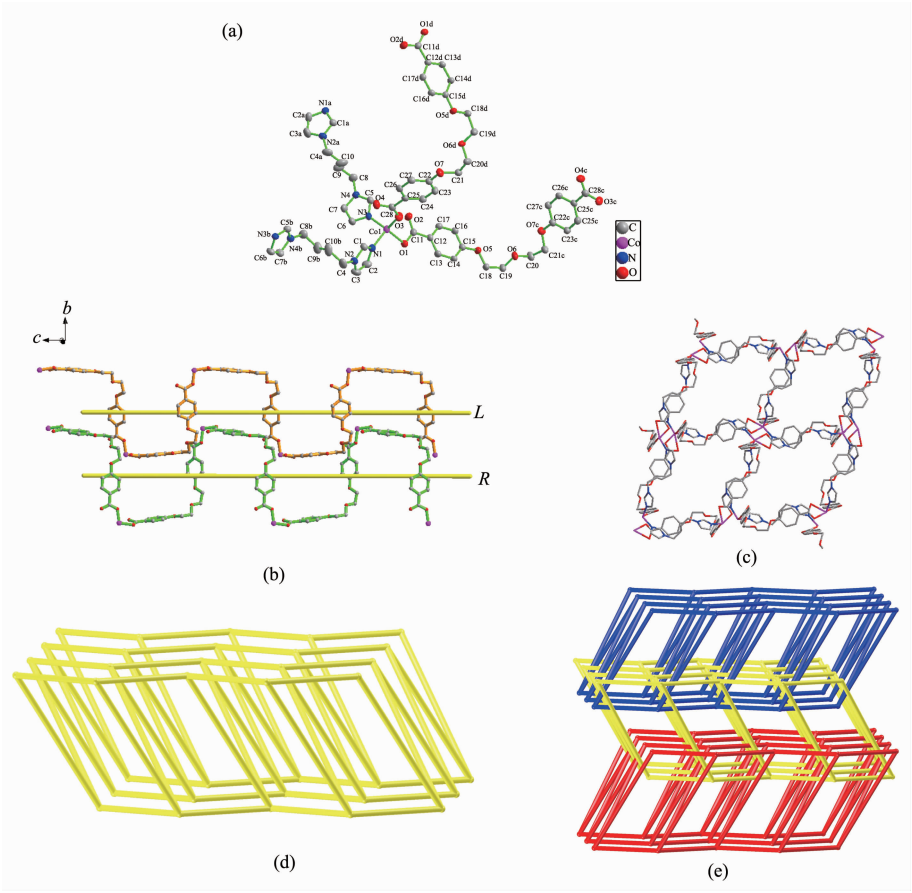

In (a): The atoms are drawn at the 30% probability level; Symmetry codes: a: 0.5+*x*, *y*, 0.5−*z*; b: −0.5+*x*, *y*, 0.5−*z*; c: 1.5−*x*, 1−*y*, 0.5+*z*; d: 1.5−*x*, 1−*y*, −0.5+*z*; The hydrogen atoms and lattice water molecule are omitted for clarity

Fig.1　(a) Coordination environment of the Co(Ⅱ) ion in **1**; (b) The infinite 1D left and right helical chains formed by Co1 centers and L ligands; (c) View of the 2D framework of **1** along the *b* axis; (c) Schematic illustrating the 2D 4-connected **sql** network in **1**; (d) Schematic representation of the 2D→2D 3-fold interpenetrating net in **1**

orthorhombic space group $P2_12_12_1$. The asymmetric unit consists of two independent Co(Ⅱ) ions, two L ligands and two bbix ligands. As shown in Fig.2a, each Co(Ⅱ) ion is coordinated by two nitrogen atoms from two different bbix ligands, and two carboxylic oxygen atoms from two different L ligands, forming a distorted CoO_2N_2 tetrahedral geometry. In **2**, the Co-O bond lengths range between 0.194 2(5) and 0.197 0(4) nm, and the Co-N distances are 0.201 5(5) and 0.202 5(5) nm, both of which are in the normal range.

The completely deprotonated L ligand acts as a μ_2-bridge linking two Co(Ⅱ) ions, which is similar to **1**. Differently, the carboxylate groups of the L ligand link the Co(Ⅱ) centers into an infinite 1D "S"-like chain, which contains a Co⋯Co separation of 2.006 80(26) nm. Each bbix ligand connects two neighboring cobalt atoms to give a zigzag chain. The overall 3D framework is formed by the intersection at the shared Co(Ⅱ) nodes (Fig.2b).

A better insight into the nature of this 3D framework can be provided by a topology analysis. The 3D structure of **2** can be clarified as a classical diamond (**dia**) lattice by considering Co(Ⅱ) ions as the 4-connected nodes and all ligands as the linkers (Fig. 2c). Notably, the large channel in a single framework has an approximate pore size of 1.366 nm×2.095 nm, which allows the other five identical 3D single frameworks to penetrate and, thus, affords a 6-fold interpenetrating architecture (Fig.2d).

2.3 Thermogravimetric analysis and PXRD

In order to further investigate the thermal stability of the complexes, the thermogravimetric analyses (TGA) of the two complexes were performed on the single crystal samples in a nitrogen atmosphere with a heating rate of 5 ℃·min^{-1} (Fig.3). For complex **1**, the weight loss of 2.2% from about 50 to 170 ℃ is attributed to the loss of one free water molecule (Calcd. 2.7%).

There is no further weight loss from 170 to 305 ℃, and after that temperature, the organic components start to decompose. The TGA study of **2** shows no weight loss from room temperature to 325 ℃, indicating the better thermal stability of the framework. Above 325 ℃, a rapid weight loss is

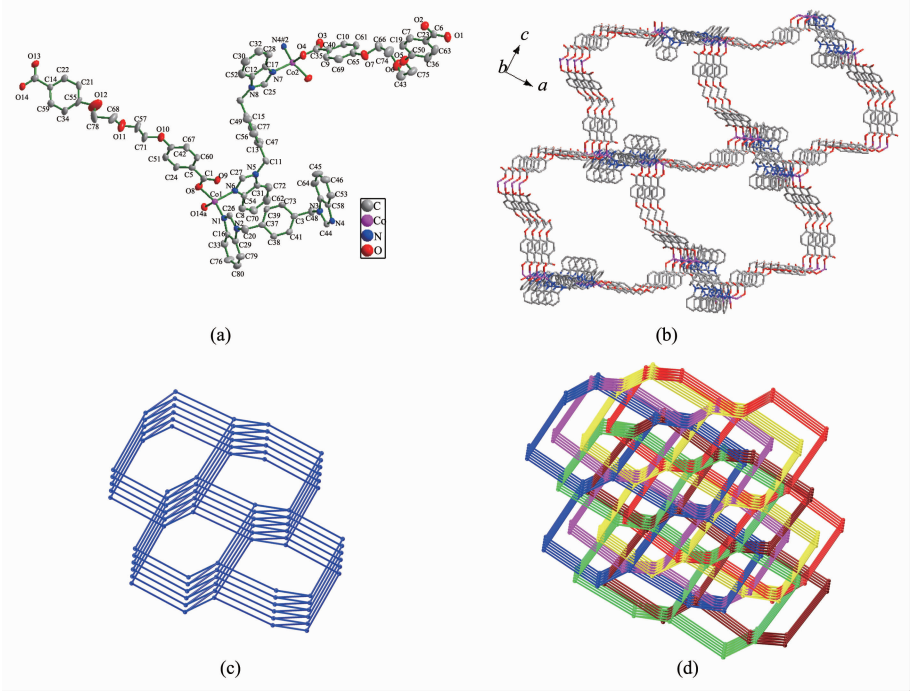

In (a): The atoms are drawn at the 30% probability level; Symmetry codes: a: −0.5−x, −y, 0.5+z; b: x, −1+y, z; The hydrogen atoms are omitted for clarity

Fig.2 (a) Coordination environment of the Co(Ⅱ) ions in **2**; (b) View of the 3D framework of **2** along the b axis; (c) Schematic illustrating the 3D **dia** topology in **2**; (d) Schematic representation of the 6-fold interpenetrating diamond net in **2**

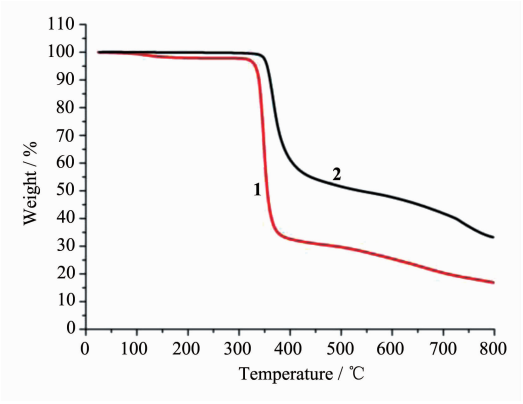

Fig.3　TGA curves of complexes **1** and **2**

observed which can be attributed to the burning of the organic ligands.

In order to check whether the crystal structures are truly representative of the bulk materials, the powder X-ray diffraction (PXRD) experiments were carried out for **1** and **2** at room temperature. As shown in Fig.4, the peak positions of the simulated and experimental PXRD patterns are in agreement with each other, demonstrating that the bulk synthesized materials and the measured single crystals are the same.

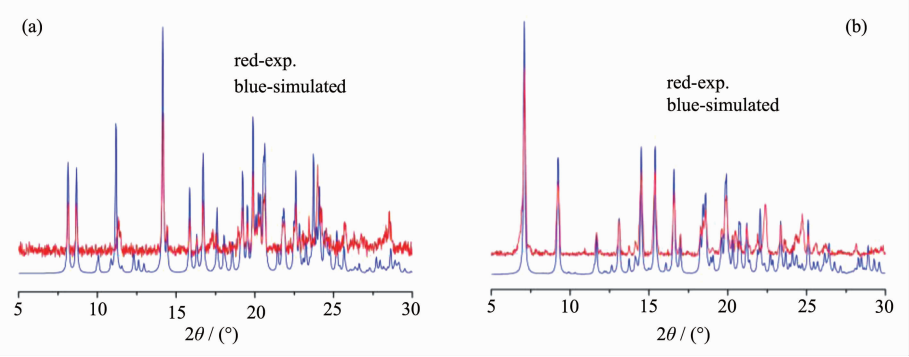

Fig.4　PXRD patterns of **1** (a) and **2** (b)

2.4　Magnetic Properties

The temperature-dependent magnetic susceptibility data of complexes **1** and **2** have been measured for polycrystalline samples at an applied magnetic field of 1 000 Oe in the temperature range of 2~300 K. The $\chi_M T$ vs T curves are shown in Fig.5. At 300 K, the $\chi_M T$ values for the two complexes are 2.45 and 2.32 $cm^3 \cdot K \cdot mol^{-1}$, respectively, considerably higher than expected value of 1.875 $cm^3 \cdot K \cdot mol^{-1}$ for one magnetism-isolated Co(Ⅱ) ion with S=3/2 and g=2.0, and they are common values for high-spin complexes with tetrahedral Co(Ⅱ) centers (2.312~3.381 $cm^3 \cdot K \cdot mol^{-1}$)[20]. The magnetic behavior can be attributed to a larger orbital contribution arising from the $^4A_{2g}$ ground-state of Co(Ⅱ) ions (commonly found for Co(Ⅱ) ions) [19]. The $\chi_M T$ values gradually decrease upon lowering the temperature to about 70 K and below this temperature falls very rapidly to reach 1.66 and 1.53 $cm^3 \cdot K \cdot mol^{-1}$ for **1** and **2** at 2 K, respectively. From the structure analysis of complexes **1** and **2**, the magnetic centers separated by the long L and the bimb or bbix coligands are weakly magnetically coupled (1.781 3 and 1.159 2 nm for **1**, 2.094 8 and 1.371 3 nm for **2**), which are very large for effective magnetic exchange among the paramagnetic centers. Therefore, the effects of the non-quenched orbital contribution for the Co(Ⅱ) ions are probably responsible for the gradual decrease of the $\chi_M T$ values on lowering the temperature. The plot of $1/\chi_M$ versus T can be fitted by the Curie-Weiss law ($\chi_M = C/(T-\theta)$) in

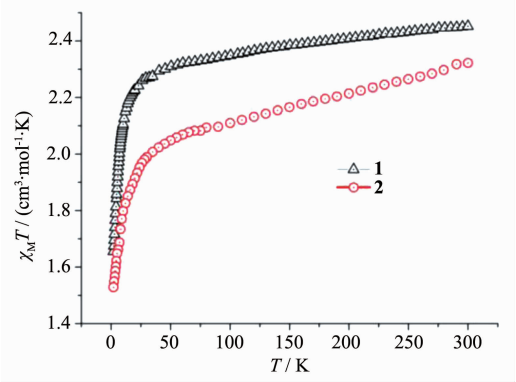

Fig.5　Plots of the temperature dependence of $\chi_M T$ at 1 000 Oe for complexes **1** and **2**

the range of 2~300 K, giving the Curie constant value C=2.45 and 2.29 $cm^3 \cdot K \cdot mol^{-1}$, Weiss constant θ=−2.30 and −4.63 K for **1** and **2**, respectively. The Curie constant values are consistent with the $\chi_M T$ values at room temperature. The negative values of θ further confirm the antiferromagnetic behaviors of complex **1** and **2**.

3 Conclusions

In summary, we successfully synthesized two new Co(Ⅱ) complexes with different topologies and varying levels of interpenetration from a rare flexible dicarboxylate acid and different imidazole-based ligands. Complex **1** shows a 2D→3D uninodal 4-connected **sql** net with 3-fold interpenetration; complex **2** shows a 3D 4-connected framework of 6^6 **dia** topology with 6-fold interpenetration. The results demonstrate that the structural motifs and degree of interpenetration of the Co(Ⅱ) coordination networks can be tuned by changing the shapes of the imidazole-based coligands. The magnetic properties of the two complexes indicate the typical antiferromagnetic interactions between the adjacent Co(Ⅱ) ions.

References:

[1] Jiang H L, Makal T A, Zhou H C. *Coord. Chem. Rev*., **2013**,**257**:2232-2249

[2] He W W, Li S L, Zang H Y, et al. *Coord. Chem. Rev*., **2014**,**279**:141-160

[3] Elsaidi S K, Mohamed M H, Wojtas L, et al. *J. Am. Chem. Soc*., **2014**,**136**:5072-5077

[4] (a) Park J H, Lee W R, Kim Y, et al. *Cryst. Growth Des*., **2014**,**14**:699-704

(b) Wang Z J, Qin L, Zhang X, et al. *Cryst. Growth Des*., **2015**,**15**:1303-1310

(c) Ju P, Jiang L, Lu T B. *Inorg. Chem*., **2015**,**54**:6291-6295

[5] (a) Batten S R, Robson R. *Angew. Chem. Int. Ed*., **1998**,**37**:1460-1494

(b) Batten S R. *CrystEngComm*, **2001**,**3**:67-73

(c) Carlucci L, Ciani G, Proserpio D M. *Coord. Chem. Rev*., **2003**,**246**:247-289

[6] Shi P F, Xiong G, Zhao B, et al. *Chem. Commun*., **2013**,**49**:2338-2340

[7] Rowsell J L C, Yaghi O M. *Angew. Chem. Int. Ed*., **2005**,**44**:4670-4679

[8] Ren C X, Zheng A L, Cai L X, et al. *CrystEngComm*, **2014**,**16**:1038-1043

[9] Chen P K, Batten S R, Qi Y, et al. *Cryst. Growth Des*., **2009**, **9**:2756-2761

[10]Miller J S. *Adv. Mater*., **2001**,**13**:525-527

[11]Chu Q, Su Z, Fan J, et al. *Cryst. Growth Des*., **2011**,**11**:3885-3894

[12]Sun G M, Luo F, Song Y M, et al. *Dalton Trans*., **2012**,**41**:11559-11561

[13]Qi Y, Che Y X, Batten S R, et al. *CrystEngComm*, **2008**,**10**:1027-1030

[14]Lan Y Q, Li S L, Qin J S, et al. *Inorg. Chem*., **2008**,**47**:10600-10610

[15]Qi Y, Li Y H, Wang Y Z. *Anorg. Allg. Chem*., **2013**,**639**:2258-2262

[16]Wang Y, Qi Y, Li Q, et al. *Polyhedron*, **2015**,**87**:237-244

[17](a) Wen L L, Lu Z D, Lin J G, et al. *Cryst. Growth Des*., **2007**,**7**:93-99

(b) Li L L, Li H X, Ren Z G, et al. *Dalton Trans*., **2009**,**40**:8567-8573

[18]Sheldrick G M. *SHELXL*-97, *Programs for the Refinement of Crystal Structure*, University of Göttingen, Göttingen, Germany, **1997**.

[19](a) Wang Y, Zhao F H, Shi A H, et al. *Inorg. Chem. Commun*., **2012**,**20**:23-26

(b) Liu Y Y, Ma J F, Yang J, et al. *Inorg. Chem*., **2007**,**46**:3027-3037

(c) Ma L F, Wang L Y, Wang Y Y, et al. *Inorg. Chem*., **2009**,**48**:915-924

[20](a) Zhou H, Liu G X, Wang X F, et al. *CrystEngComm*, **2013**,**15**:1377-1388

(b) Mukherjee S, Samanta D, Mukherje P S. *Cryst. Growth Des*., **2013**,**13**:5335-5343